


Opposite current-induced spin polarizations in bulk-metallic Bi_2Se_3 and bulk-insulating $\text{Bi}_2\text{Te}_2\text{Se}$ topological insulator thin flakes

Jifa Tian ^{1,2,3,*}, Cüneyt Şahin,⁴ Ireneusz Miotkowski,¹ Michael E. Flatté ⁴ and Yong P. Chen^{1,2,5,6,7,8}

¹*Department of Physics and Astronomy, Purdue University, West Lafayette, Indiana 47907, USA*

²*Birck Nanotechnology Center, Purdue University, West Lafayette, Indiana 47907, USA*

³*Department of Physics and Astronomy, University of Wyoming, Laramie, Wyoming 82071, USA*

⁴*Optical Science and Technology Center and Department of Physics and Astronomy, University of Iowa, Iowa City, Iowa 52242, USA*

⁵*Purdue Quantum Science and Engineering Institute, Purdue University, West Lafayette, Indiana 47907, USA*
and *Quantum Science Center, Oak Ridge, Tennessee 37831 USA*

⁶*School of Electrical and Computer Engineering, Purdue University, West Lafayette, Indiana 47907, USA*

⁷*Institute of Physics and Astronomy and Villum Centers for Dirac Materials and for Hybrid Quantum Materials, Aarhus University, 8000 Aarhus-C, Denmark*

⁸*WPI-AIMR International Research Center for Materials Sciences, Tohoku University, Sendai 980-8577, Japan*



(Received 21 August 2020; accepted 17 December 2020; published 14 January 2021)

One of the most fundamental and exotic properties of three-dimensional (3D) topological insulators (TIs) is spin-momentum locking (SML) of their topological surface states (TSSs), promising for potential applications in future spintronics. However, other possible conduction channels, such as a trivial two-dimensional electron gas (2DEG) with strong Rashba-type spin-orbit interaction (SOI) and bulk-conducting states that may possess a spin Hall effect (SHE), can coexist in 3D TIs, making determining the origin of the current-induced spin polarization (CISP) difficult. In this work, we directly compared the CISP between bulk-insulating $\text{Bi}_2\text{Te}_2\text{Se}$ (BTS221) and bulk-metallic Bi_2Se_3 thin flakes using spin potentiometry. In the bulk-insulating BTS221, the observed CISP has a sign consistent with the expected helicity of the SML of the TSS, but an opposite sign to its calculated bulk spin Hall conductivity. However, compared to BTS221, an opposite CISP is observed in the bulk-metallic Bi_2Se_3 , consistent with both the expectations of its Rashba-Edelstein effect of the band-bending induced 2DEG and bulk intrinsic spin Hall Effect (SHE). If one assumes a representative occupation of the Rashba band of $3 \times 10^{13} \text{ cm}^{-2}$ in Bi_2Se_3 with a relevant relaxation time of 100 fs, the contribution to the CISP could be more dominated by the bulk intrinsic SHE. Our results provide an electrical way to distinguish the TSS from other possible conducting channels in spin transport measurements on 3D TIs, and open ways for the potential applications in charge-spin conversion devices.

DOI: [10.1103/PhysRevB.103.035412](https://doi.org/10.1103/PhysRevB.103.035412)

I. INTRODUCTION

Charge carriers in materials with strong spin-orbit interaction (SOI) commonly experience a momentum-dependent effective magnetic field and a geometric phase [1–3]. These features are particularly attractive for the realization of device concepts in which spin polarization is generated from a charge current, manipulated by electric fields, and detected electrically or optically [3]. Three-dimensional topological insulators (3D TIs) possess nontrivial spin-momentum locked topological surface states (TSSs) representing a new type of the SOI. The charge carriers of TSS are massless Dirac fermions with their spins locked in plane and perpendicular to their momentum [Fig. 1(a)] [4–10], making the TI system a promising source for generating spin polarization and spin current without ferromagnetic (FM) materials. However, real 3D TI materials can also host trivial 2D electron gas (2DEG) with strong Rashba-type SOI near the surfaces derived from their bulk states [Fig. 1(a)] [11, 12]. These Rashba 2DEGs typically have two Fermi surfaces [Fig. 1(a)] with opposite spin

helicities, where the outer one (which contributes more to the transport than the inner one [13]) has the opposite spin helicity compared to that of TSS [11, 12]. Furthermore, the bulk of many 3D TIs may be doped to be conducting, and can possess a spin Hall effect [SHE, Fig. 1(a)] resulting from the heavy elements present. In recent years, spin potentiometry has been applied to study current-induced spin polarization (CISP) in 3D TIs, where the direction of spin polarization can be determined from a voltage difference (thus a spin chemical potential difference) measured between opposite magnetizations of an FM tunneling probe, controlled by an in-plane magnetic field applied along its easy axis [14–21]. However, so far, most of the reported CIPs measured on different 3D TIs have been solely ascribed to TSS, even though some of the spin signals (voltage differences) show opposite signs [14–23]. Especially, the contributions to CISP from Rashba 2DEG and bulk intrinsic SHE in 3D TIs have been largely ignored. Thus, to clarify the origins of the CISP in 3D TIs, a careful study considering all the possible contributions is desired.

In this work, we systematically studied and compared the CIPs in bulk-insulating $\text{Bi}_2\text{Te}_2\text{Se}$ (BTS221) and bulk metallic Bi_2Se_3 TI thin flakes by spin potentiometry. The spin devices [Figs. 1(b) and 1(c)] of the two materials were made

*jtian@uwyo.edu

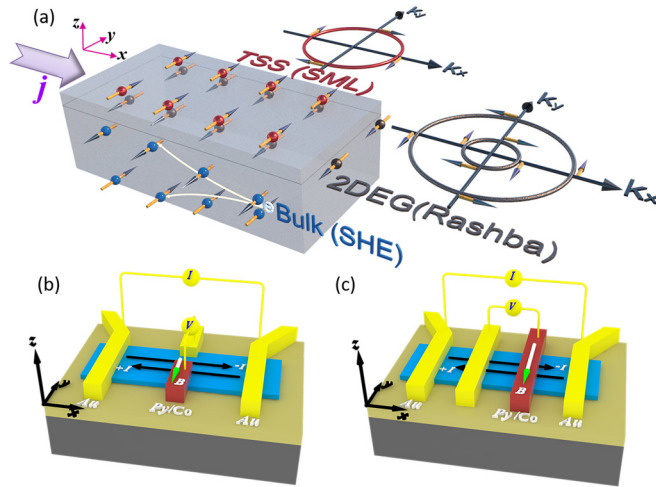


FIG. 1. Schematic illustrations of possible states that could give current-induced spin polarization on surfaces of 3D topological insulator materials and the circuit layout used in the spin potentiometric measurements. (a) Schematic illustration of topological surface state, band-bending induced Rashba-type two-dimensional electron gas near the top surface, and bulk spin Hall effect in 3D TIs. The red, black, and blue spheres with arrows representing the current-induced spin polarization due to TSS, 2DEG, and bulk SHE, respectively. The schematics of the Fermi surface of TSS (in red) and Rashba 2DEG (in gray) are shown in (a). Schematic device structures and circuit layouts used in the spin potentiometric measurements: (b) Hall-probe like and (c) four-terminal geometries. The TI surface defines the x - y plane and the surface normal z direction. The two outside nonmagnetic (e.g., Au) contacts are used to apply a dc bias current (I), and the middle ferromagnetic (e.g., Py or Co) contact is magnetized by an in-plane magnetic field B along its easy axis (y , with $-y$ defining the positive B and positive M directions).

using a similar nanofabrication process and measured in the same system. The FM tunneling probe detects the CISP on the top surface. In both materials, we observed a similar steplike spin signal when an in-plane magnetic field is applied to switch the magnetization of the FM voltage probe (the spin detector), and reversing the current direction reverses the sign of the spin signal. The CISP in bulk-insulating BTS221 is found to be consistent with the theoretical expectations of TSS, whereas the CISP measured in bulk-metallic Bi_2Se_3 is opposite, and is consistent with the Rashba-Edelstein effect from the band-bending induced 2DEG near the top surface. We further studied the back gating, current, and temperature dependences of the spin signals measured in these two materials. Furthermore, we calculated the bulk intrinsic SHC of Bi_2Se_3 and BTS221, and discussed its possible contribution to the observed CISP. Our work clarifies and highlights the differences in spin transport from TSS, Rashba 2DEG, and bulk SHE, and enables the potential applications in spintronics by utilizing these states in 3D TIs.

II. EXPERIMENTAL METHODS

High-quality BTS221 and Bi_2Se_3 single crystals were grown by the Bridgman method [18,24,25]. The 3D TI thin flakes (with a typical thickness of ~ 10 – 40 nm, and lateral size up to ~ 5 – 10 μm) were exfoliated from these bulk crystals

and placed on top of SiO_2 (thickness 285 nm)/Si (heavily doped) substrates serving as the back gate. The BTS221 crystal is bulk insulating [18], while the Bi_2Se_3 crystal is heavily n -type doped (presumably due to the Se vacancies [24]). The spin devices of the two materials were fabricated using a similar process as reported in our previous work [18]. For fabricating the spin devices, we used both the permalloy (Py, $\text{Ni}_{0.80}\text{Fe}_{0.20}$) and cobalt (Co) as the FM probes (the spin potentiometer), separated from the TI surface by 1-nm-thick Al_2O_3 . The nonmagnetic contacts are Au [Figs. 1(b), 1(c), 2(a), and 2(d)].

Two circuit layouts [Hall-bar-like and four-terminal configurations, schematically shown in Figs. 1(b) and 1(c), respectively] were used in the spin potentiometric measurements on both the BTS221 and Bi_2Se_3 devices. A dc current was applied between two “outmost” Au electrodes and a voltage (V) was measured between an FM (Co or Py) and the adjacent Au contacts using a high-impedance voltmeter. We define a positive current ($+I$) as flowing from right to left along the $-x$ direction (thus the electrons flow from left to right along the $+x$ direction), and a positive in-plane magnetic field ($+B$) as applied in the $-y$ direction along the easy axis of the FM electrode (so its majority spin points to the $+y$ direction) [18]. A voltage difference (spin signal) δV can be extracted when the magnetization of the FM tunneling probe is reversed. We note that the sign of the spin signal and the CISP for a given current are independent of the choices of the circuit layout and the FM contacts. All measurements were performed in a variable-temperature cryostat with a base temperature (T) of 1.5 K.

III. RESULTS AND DISCUSSION

A. CISP in BTS221 and Bi_2Se_3 3D TI samples

We directly compared the spin transport results measured on a 40-nm-thick BTS221 [device A, Fig. 2(a)] and a 35-nm-thick Bi_2Se_3 [device B, Fig. 2(d)]. For the bulk-insulating BTS221 sample, the voltages (ΔV) measured between a Py spin detector (contact “2” in device A) and an adjacent Au contact (“3”) as a function of the in-plane magnetic field (B) are detailed in Figs. 2(b) and 2(c), where a linear background has been subtracted (Fig. S1 in the Supplemental Material [26]). We see a high- (low-) voltage state when the channel spin polarization s is parallel (antiparallel) to the direction of the magnetization M of the FM contact (equivalently, when the FM majority spins, which are oriented opposite to M , are antiparallel (parallel) to the channel spin polarization s , the FM contact measures the lower (higher) electrical chemical potential μ of the less (more) occupied channel spin states). We note that the voltage V has a direct relationship with the electrical chemical potential μ of $V = \mu/q$, where charge $q = -e$ if the charge carriers are electrons. The sign of the measured spin signal $\delta V (= \Delta V_{+M} - \Delta V_{-M})$ can be extracted and used to determine the direction of CISP [18,22]. As shown in Fig. 2(b), when a positive bias current I is applied along the $-x$ direction and the magnetization M of the Py detector is in the $-y$ ($+y$) direction, we observed a high- (low-) voltage state with a spin signal $\delta V \sim 20$ μV . Thus, we can determine that the direction of the spin polarization s in the

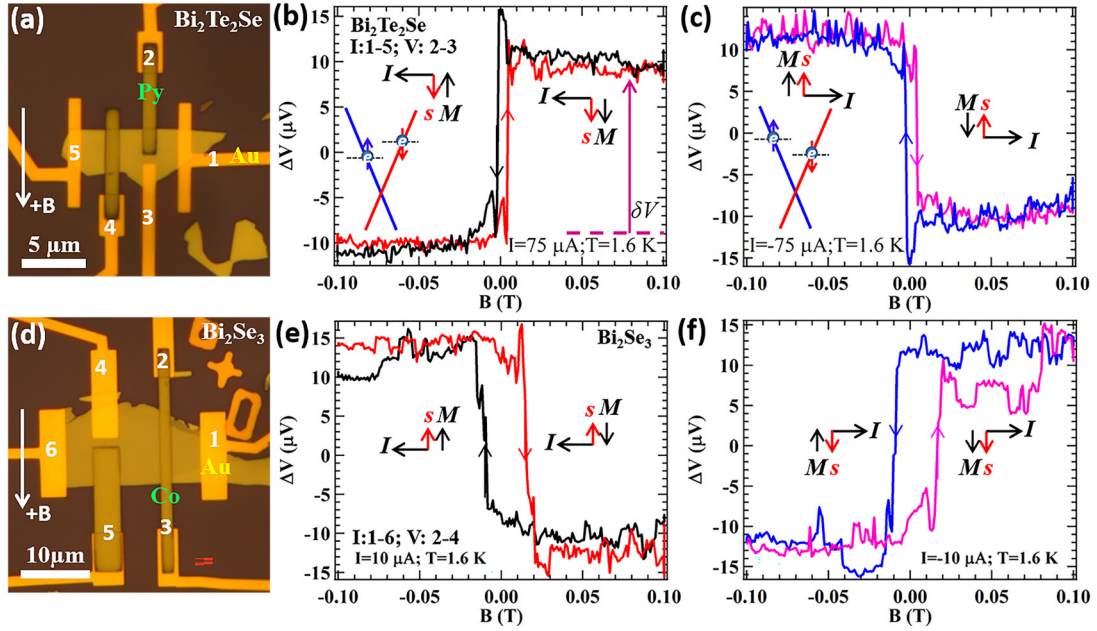


FIG. 2. Current-induced spin polarizations with opposite signs in bulk-insulating $\text{Bi}_2\text{Te}_2\text{Se}$ (BTS221) and bulk-metallic Bi_2Se_3 thin flakes. (a) Optical image of a typical BTS221 device (device A, a 40-nm-thick flake). The corresponding circuit layout is shown in Fig. 1(b). (b), (c) Voltage (ΔV) measured by an FM (Py, electrode “2”) spin detector as a function of the in-plane magnetic field (B) at bias currents $I = 75 \mu\text{A}$ (b), and $-75 \mu\text{A}$ (c), where a linear background has been subtracted from all the traces. The purple arrow represents the extracted spin signal $\delta V = \Delta V_{+M} - \Delta V_{-M}$. Here, ΔV_{+M} and ΔV_{-M} are the representative voltages measured before and after the magnetization switching of the FM spin detector near the coercive field. Insets of (b), (c) are the schematic band structures of TSS under positive and negative bias currents, respectively. (d) Optical image of a representative Bi_2Se_3 device (device B, a 35-nm-thick flake). (e), (f) Voltage (ΔV) measured by a Co (electrode “2”) spin detector as a function of the in-plane B field at bias currents $I = 10 \mu\text{A}$ (e), and $-10 \mu\text{A}$ (f). The raw data of the voltage traces are vertically shifted to be centered at zero. For (b), (c), (e), and (f), the directions of the bias current I , current-induced spin polarization s at the top surface (inferred from the sign of the spin signal), and magnetization M of the FM are labeled by the corresponding arrows. The arrows on the data traces indicate magnet field sweep directions. All the measurements were performed at $T = 1.6 \text{ K}$.

bulk-insulating BTS221 flake is along the $-y$ direction (red arrow) for a positive I along the $-x$ direction (electron momentum along the $+x$ direction), such that a $+y$ -magnetized detector (majority spins along $-y$) would detect a high occupation or chemical potential (thus low voltage). As expected, reversing the bias current ($I = -75 \mu\text{A}$) reverses the sign of the spin signal [now $\delta V \sim -20 \mu\text{V}$ in Fig. 2(c)] and the corresponding channel spin polarization s . From the above analyses, we conclude that the CISP in the bulk-insulating BTS221 is consistent with the expectation of TSS due to SML [18,19,21,27]. In stark contrast, for the bulk-metallic Bi_2Se_3 [Fig. 2(d), device B], a low- (high-) voltage state is observed at the positive (negative) magnetization M along $-y$ ($+y$) and a positive $I = 10 \mu\text{A}$ along $-x$ [Fig. 2(e)], showing an opposite trend of the hysteretic steplike spin signal ($\delta V < 0$) comparing to that of BTS221. Reversing current I to $-10 \mu\text{A}$ reverses the trend of the spin signal ($\delta V > 0$) [Fig. 2(f)]. Given the same sign of the bias current I (Fig. 2), the opposite spin signal observed in Bi_2Se_3 compared to that of BTS221 indicates an opposite CISP (the red arrows in Fig. 2) and a non-TSS origin. We note that the measured spin signal and the direction of the CISP in bulk-metallic Bi_2Se_3 samples are consistent with that of the molecular-beam epitaxy (MBE)-grown Bi_2Se_3 previously reported [14]. As demonstrated by the spin-resolved angle-resolved photoemission spectroscopy (ARPES) [11,12], the spin helicity of the outer Fermi surface

of the Rashba 2DEG in Bi_2Se_3 is opposite to that of TSS, suggesting that the Rashba 2DEG [13] can be one of the causes for the observed opposite CISP in Bi_2Se_3 . In addition, we will also discuss possible contribution of bulk spin Hall effect as another possible cause in Sec. III D.

B. Current, temperature, and gate dependences of the spin signals for BTS221

We studied the current and temperature dependences of the spin signals for BTS221 (device A). Figure 3(a) shows the voltage measured by the Py spin detector as a function of the in-plane B field at different bias currents ranging from ± 0.5 to $\pm 100 \mu\text{A}$ at $T = 1.6 \text{ K}$. To highlight the current dependence of the spin signal, all of the curves have been vertically offset to have their central values aligned. The corresponding spin signal δV as a function of the bias current I is summarized in Fig. 3(b). We see that δV linearly increases with the applied current I , consistent with the expectations of CISP [13]. The temperature-dependent spin signals were measured at bias currents $I = \pm 100 \mu\text{A}$. The amplitude of the spin signal $|\delta V|$ shows a weak dependence on temperature when T is below 60 K. However, when T is above 60 K, $|\delta V|$ decreases steadily and vanishes at $\sim 120 \text{ K}$. After comparing the temperature dependence of the spin signal with that of the sample resistance R (Fig. S2 in the Supplemental Material

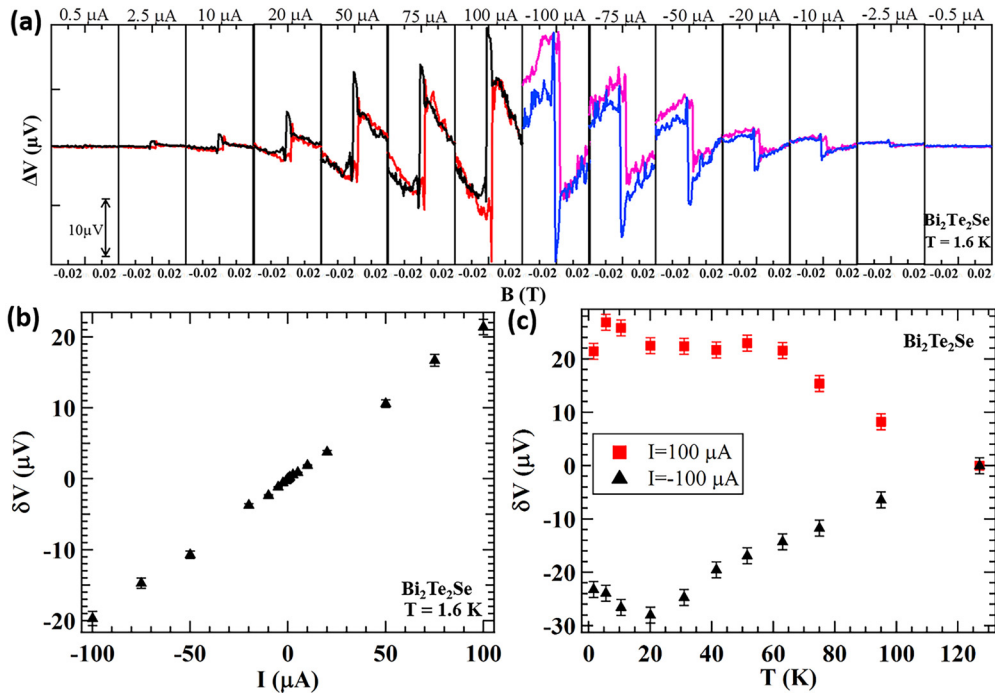


FIG. 3. Current and temperature dependences of the spin signal measured on bulk-insulating BTS221. (a) The voltage measured by the Py spin detector on device A as a function of the in-plane magnetic field at different bias currents. The voltage traces have been vertically offset to have their central values aligned. (b) The spin signal δV as a function of the applied bias current. All the measurements are performed at $T = 1.6 \text{ K}$. (c) The spin signal δV as a function of temperature ranging from 1.6 to 125 K measured at a bias current of $+100$ or $-100 \mu\text{A}$.

[26]), we find that, similar to the temperature-dependent spin signal, R changes its trend at $\sim T = 60 \text{ K}$, suggesting that the bulk conduction becomes notable when T is $> 60 \text{ K}$. We note that the reduction and disappearance of the spin signal at higher temperatures may be attributed to various factors, such as the increased contributions from the bulk states, increased scattering (due to phonons) and thermal fluctuations of the polarized spins [16], and degradation of the quality of Al_2O_3 tunneling barriers [21], etc.

We further studied the gate dependence of the spin signal measured on the bulk-insulating BTS221 sample (Fig. 4). The representative spin signals measured on device A at different gate voltages (V_g) are shown in Fig. 4(a), where the spin results measured at a bias current of $+20 \mu\text{A}$ ($-20 \mu\text{A}$) are shown in the top (bottom) panel. We note that all the voltage traces have been vertically offset to have their central values aligned. The gate dependence of the spin signal δV is summarized in Fig. 4(b), where the spin signal $|\delta V|$ is enhanced by ~ 3 times as V_g is tuned from 80 to -80 V . Such an enhancement is consistent with the gate dependence of the voltage (V_0) measured at $B = 0 \text{ T}$ and a bias current of $I = 20 \mu\text{A}$ as shown in Fig. 4(c), where V_0 can be tuned with an on-off-ratio of ~ 4 , confirming a strong back-gate effect of our BTS221 device. We further note that the qualitative trends of the gate-dependent spin signal (δV increases as the Fermi level is tuned to approach the Dirac point) as well as the CISP are consistent with the experimental results measured on bulk-insulating $(\text{Bi}, \text{Sb})_2\text{Te}_3$ thin films grown on the SrTiO_3 (with a high dielectric constant at low temperatures) substrates where an ambipolar field effect has been achieved [21].

C. Current and temperature dependences of the spin signals for Bi_2Se_3

In order to have a better understanding of the opposite spin helicity observed in the bulk-metallic Bi_2Se_3 , we systematically studied the current and temperature dependences of the spin signal. Figure 5(a) shows the spin signal (measured on device B) as a function of the in-plane magnetic field at different bias currents ranging from ± 0.05 to $\pm 100 \mu\text{A}$ at $T = 1.6 \text{ K}$. The extracted spin signal δV (negative for $+I$ and positive for $-I$) as a function of I is summarized in Fig. 5(b), where $|\delta V|$ linearly increases with the increasing bias current at $|I| < 20 \mu\text{A}$ but saturates (possibly due to Joule heating) at high currents ($|I| > 20 \mu\text{A}$). The temperature dependence of the spin signals measured at $I = \pm 15 \mu\text{A}$ is summarized in Fig. 5(c). We see that, different from BTS221, as the temperature increases, the spin signal δV of Bi_2Se_3 quickly decreases and disappears at $\sim 80 \text{ K}$. Other than the above-listed possible factors for BTS221, the quick reduction of the spin signal in Bi_2Se_3 can be consistent with the expectations of Rashba-Edelstein effect from the 2DEG [13] since its CISP reduces much faster than that of TSS as temperature increases (possibly reflecting the relative proximity to other states that can be thermally excited).

D. Origin of the CISP in BTS221 and Bi_2Se_3

Depending on the location of the Fermi level, different electronic states and mechanisms, such as TSS, Rashba 2DEG, and the bulk SHE, can contribute to the measured CISP in 3D TIs. We can infer that the Fermi level in BTS221 is located in the TSS based on its temperature dependence

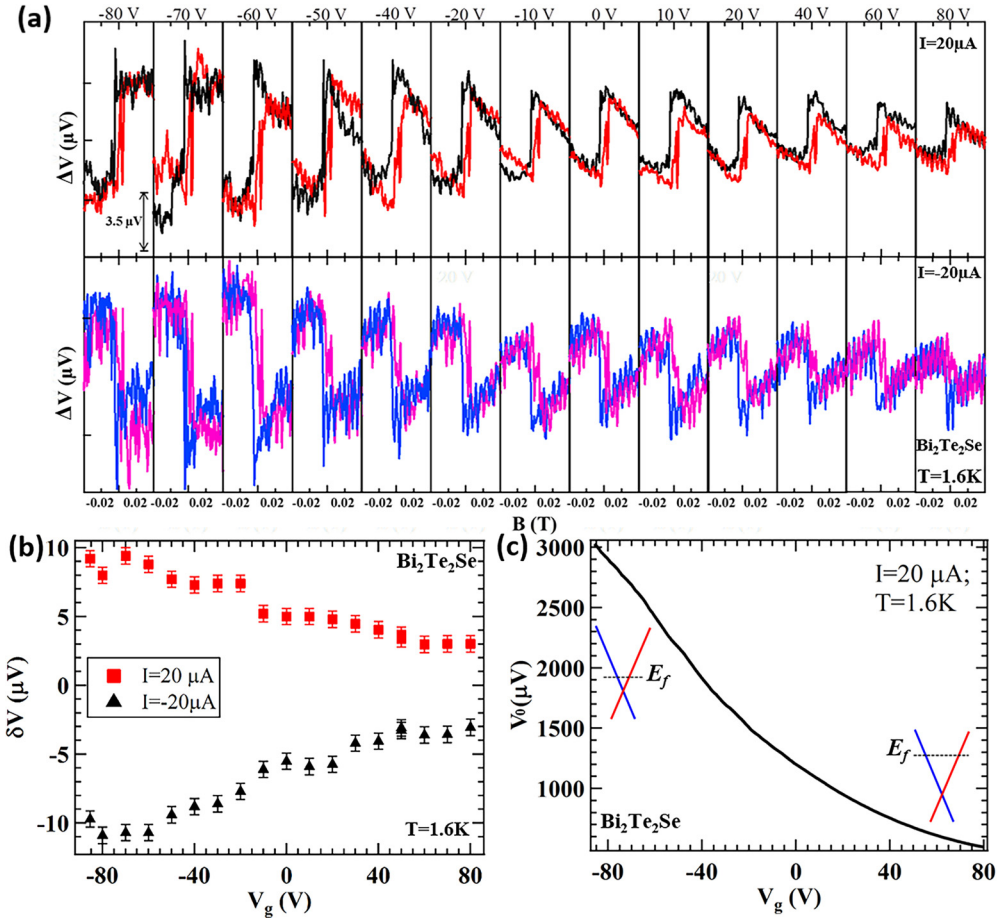


FIG. 4. Gate dependence of the spin signal measured on the bulk-insulating BTS221. (a) The voltage measured by the Py spin detector on device A as a function of the in-plane magnetic field at different back-gate voltages (V_g) and bias currents of $20 \mu\text{A}$ (top panels) and $-20 \mu\text{A}$ (bottom panels), respectively. The voltage traces have been vertically offset to have their central values aligned. (b) Spin signal δV as a function of V_g for both positive (red squares) and negative (black triangles) bias currents. (c) Back-gate dependence of the voltage (V_0) measured between electrodes “2” and “3” at zero B field at a bias current of $I = 20 \mu\text{A}$ applied between electrodes “1” and “5.” Insets are the schematics of the band structure of TI with the corresponding Fermi levels at the most positive and negative gate voltages. All the measurements were performed at $T = 1.6 \text{K}$.

of the resistance R [Fig. S2(a) in the Supplemental Material [26], exhibiting a weakly insulating behavior for $T > 60 \text{K}$] and the extracted (including carriers from both the top and bottom surfaces) 2D carrier density of $\sim 1 \times 10^{13} \text{cm}^{-2}$ (Fig. S2 in the supplemental Material [26]), because the maximum carrier density of TSS at the bottom of the bulk conduction band for *each* surface in BTS221 is $\sim 1 \times 10^{13} \text{cm}^{-2}$ calculated based on the band structure measured by ARPES [24]. Together with their current and temperature dependences of the spin signals (Fig. 3) and its calculated bulk intrinsic SHC [Fig. 6(b), discussed below], we can conclude that the observed CISP in our bulk-insulating BTS221 is mainly due to SML of TSS [18,21]. As for Bi_2Se_3 , its Fermi level is located in the bulk conduction band [28] because of its clearly metallic behavior (Fig. S2(d) in the Supplemental Material [26]) and the high 2D carrier density ($\sim 7 \times 10^{13} \text{cm}^{-2}$, ~ 7 times higher than that of BTS221, Fig. S2(f) in the Supplemental Material [26]), since the maximum carrier density of TSS for each surface in Bi_2Se_3 is $\sim 8.9 \times 10^{12} \text{cm}^{-2}$ calculated based on the ARPES-measured band structure [29]. Thus, the measured CISP (with opposite sign compared to that of

BTS221) has little contribution from the SML of TSS, but comes from other possible states with opposite spin helicity, such as the Rashba-Edelstein effect from the band-bending induced 2DEG near the top surface, where its outer Fermi circle features an opposite spin helicity (demonstrated by the spin-resolved ARPES [11,12]) compared to that of TSS.

In addition to SML of TSS and Rashba-Edelstein effect of the Rashba-type 2DEG as the possible causes for the CISP in 3D TIs, here we discuss another possible source arising from the bulk intrinsic SHE [30] of Bi_2Se_3 and BTS221. A tight-binding Hamiltonian consisting of s - and p orbitals of the Bi, Te, and Se atoms has been constructed, including SOI with parameters taken from an earlier study [31]. We calculated the intrinsic SHC of the Bi_2Se_3 and BTS221 crystals in terms of a spin current-charge current response function within the linear response theory using the Kubo formula [32]. The SHC is the sum of the Berry curvatures of the filled bands up to the Fermi level. We computed the energy-dependent density of Berry curvatures which allows us to determine the SHC, σ_{ij}^k , as a function of the chemical potential, where i , j , and k stand for the direction of the spin current, the direction of the charge

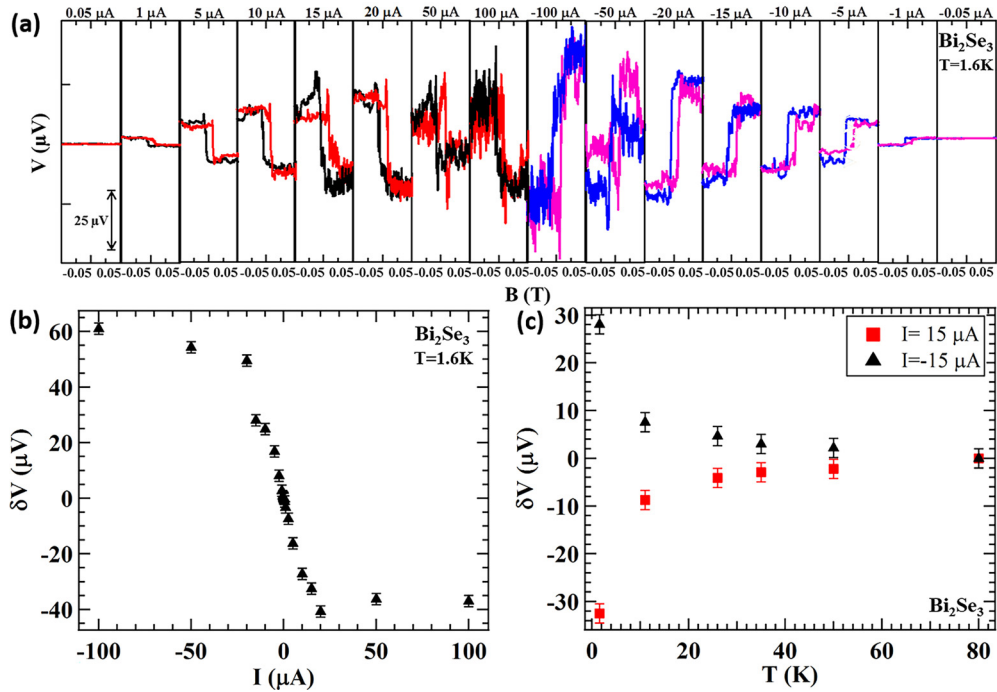


FIG. 5. Current and temperature dependences of the spin signal measured on bulk-metallic Bi_2Se_3 . (a) The voltage measured by a Co spin detector on device B as a function of the in-plane magnetic field at different bias currents, where the voltage traces have been vertically offset to have their central values aligned. (b) The spin signals δV as a function of the applied bias current I . All the measurements were performed at $T = 1.6$ K. (c) The spin signal δV as a function of the temperature ranging from 1.6 to 80 K.

current, and polarization of the spin, respectively. The coordinates used in the calculation are shown in Fig. 6(a). To directly compare the theoretical and experimental results, we chose the z , x , and y axes as the directions of spin current, charge current, and spin polarization. We summarized the calculated SHC, σ_{zx}^y , as a function of Fermi energy E_F in Fig. 6(b). The results for the SHC over the entire energy range for these materials are shown in Fig. S5 of the Supplemental Material [26]. We do not observe a significant anisotropy in the SHC results for different directions, especially for Fermi levels around the band gap. This can be attributed to the rhombohedral crystal structure of these materials, which is closely related to a simple cubic structure by a slight distortion along the body

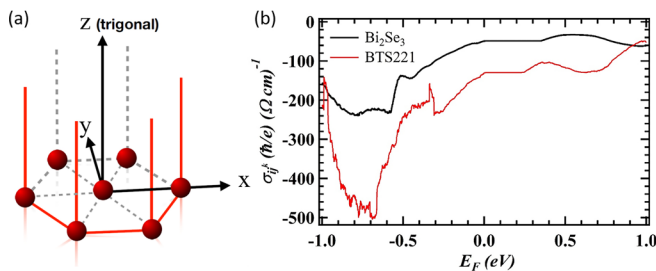


FIG. 6. The calculated intrinsic spin Hall conductivity in the bulk of Bi_2Se_3 and BTS221 . (a) The coordinate system based on the crystal structure of Bi_2Se_3 and BTS221 used in the calculations. (b) The intrinsic SHC σ_{ij}^k of Bi_2Se_3 and BTS221 crystals as a function of the Fermi energy (E_F). Here, we consider i , j , and k along the z , x , and y axes as the directions of spin current, charge current, and spin polarization, respectively.

diagonal. We can further determine the direction of CISP from the sign of the calculated SHC due to the intrinsic bulk SHE. As shown in Fig. 6(b), the negative SHC σ_{ij}^k indicates that if a charge current (electron current) flows along the $+x$ ($-x$) axis, the spin current will flow to the $+z$ axis and the induced spin polarization will point to the $-y$ axis. Based on this analysis, we can conclude that the CISP due to bulk intrinsic SHE for both Bi_2Se_3 and BTS221 would have the same sign, which would be the same as that of Rashba-Edelstein effect from the 2DEG (possibly observed in Bi_2Se_3), but opposite to that of TSS (as observed in BTS221). Thus, in Bi_2Se_3 both the intrinsic SHE and band-bending induced Rashba 2DEG can be the causes of the observed opposite CISP compared to that of BTS221 . In addition to the bulk intrinsic SHE, in Bi_2Se_3 , the extrinsic SHE due to the spin-dependent scattering (known as skew scattering) around defects (e.g., Se vacancies) may also exist. Since these Se vacancies normally create positively charged defects, electrons scattered to the top surface would have the same spin-polarization direction as that of TSS [33], resulting in the opposite sign of the spin signals measured by spin potentiometry. Thus, the skew-scattering induced SHE appears unlikely to be the cause of our observed spin signal in Bi_2Se_3 . We note a recent work on measurements of the SHC in Cr-doped $(\text{Bi}, \text{Sb})_2\text{Te}_3$ thin films using spin pumping [34] on a series of samples whose Fermi energy can be largely tuned to the valence band, the bulk energy gap, and the conduction band. We note prior experiments show that the CISP in $(\text{Bi}, \text{Sb})_2\text{Te}_3$ thin films have the same sign as what we observe in BTS221 [18,21,22]. The sign of the calculated bulk intrinsic SHC of $(\text{Bi}, \text{Sb})_2\text{Te}_3$ was found to be consistent with the spin-pumping signal measured in Cr-doped $(\text{Bi}, \text{Sb})_2\text{Te}_3$

samples [34]. The sign of the calculated SHC of $(\text{Bi, Sb})_2\text{Te}_3$ is consistent with our calculated SHC of Bi_2Se_3 and BTS221 if the same coordinate system is used. On the other hand, the facts that samples in Ref. [34] are doped with chromium and have a different composition than ours and the measurement technique is also different from ours make a proper comparison of the experiments challenging.

We may estimate the size of the effect due to the Rashba 2DEG for Bi_2Se_3 from information about the band structure of the Rashba 2DEG and measured conductivities. The measured conductivity of 10 mS (Fig. S2) per square, and assuming the geometry is roughly square with a $10\text{-}\mu\text{m}$ side (so electric field of 800 V/m and current density of 8 A/m), with a representative occupation of the Rashba band given in Ref. [12] of $3 \times 10^{13} \text{ cm}^{-2}$, corresponds to a drift velocity of 166 m/s. Assuming an approximate scattering time for the spin polarization upon current injection of about ~ 100 fs, the spin polarization should decay in less than an angstrom if carried by the Rashba 2DEG. We thus suggest that it is unlikely, based on these estimates, that the Rashba 2DEG alone would produce the spin polarization in the Bi_2Se_3 ; instead, it is likely carried by the bulk SHC. A similar estimation based on the TSS for BTS221 produces a drift velocity two orders of magnitude larger (at least), close to the Fermi velocity limit if these states were dissipationless. Thus even though the Rashba states (given a contribution to the carrier density of $3 \times 10^{13} \text{ cm}^{-2}$) appear unlikely to produce spin polarization due to carrying current, the TSS appears to do so for BTS221.

A previous report pointed out that a local Hall effect due to the fringe field of an FM detector could also induce a hysteretic steplike voltage change, which was observed in MBE-grown Bi_2Se_3 samples [28]. In our case, we have fabricated square-shaped FM detectors on both BTS221 and Bi_2Se_3 samples (Figs. S3 and S4). The representative CISP can only be detected when the applied bias current is perpendicular to the in-plane magnetic field, whereas no steplike spin signal (Figs. S3 and S4) is observed when the bias current is parallel to the magnetic field. Our results are fundamentally different from the reported fringe-field induced

steplike voltage changes [28]. Furthermore, the opposite signs of the spin signals (Fig. 2) in BTS221 and Bi_2Se_3 cannot be explained by the fringe-field induced Hall effect because both samples show n -type (which should give the same sign of the fringe-field induced Hall signal) charge carriers.

IV. CONCLUSIONS

In conclusion, we have directly compared the CISPs in bulk-insulating BTS221 and bulk-metallic Bi_2Se_3 thin flakes. We find that, for a given bias current and magnetization of the FM spin detector, the measured sign of the spin signal and the direction of the CISP in BTS221 are opposite to that of Bi_2Se_3 . The CISP observed in our bulk-insulating BTS221 can be unambiguously ascribed to TSS due to SML. The opposite spin polarization observed in our bulk-metallic Bi_2Se_3 may be more dominated by the bulk-intrinsic SHE compared to the band-bending induced Rashba 2DEG that could also contribute. Our results systematically studied the roles of different states in the observed CISP in 3D TIs, and open a potential way to manipulate spins by utilizing SML of TSS, Rashba 2DEG, and intrinsic-bulk SHE for 3D TI-based spin and nanoelectronic devices.

ACKNOWLEDGMENTS

This work was partially supported by DARPA MESO program under Award No. N66001-11-1-4107, NSF under Award No. EFMA-1641101 and Lockheed Martin Corporation. J.T. also acknowledges DOE, Office of Basic Energy Sciences, Division of Materials Sciences and Engineering for financial support under Awards No. DE-SC0020074 and No. DE-SC0021281. Y.C. also acknowledges support by the DOE Office of Science through the Quantum Science Center (QSC), a National Quantum Information Science Research Center. C.S. and M.E.F.'s theoretical analysis was supported by the Center for Emergent Materials, an NSF MRSEC under Award No. DMR-1420451.

-
- [1] Y. A. Bychkov and E. I. Rashba, Properties of a 2D electron gas with lifted spectral degeneracy, *JETP Lett* **39**, 78 (1984).
 - [2] S. LaShell, B. A. McDougall, and E. Jensen, Spin Splitting of an Au(111) Surface State Band Observed with Angle Resolved Photoelectron Spectroscopy, *Phys. Rev. Lett.* **77**, 3419 (1996).
 - [3] A. Manchon, H. C. Koo, J. Nitta, S. M. Frolov, and R. A. Duine, New perspectives for Rashba spin-orbit coupling, *Nat. Mater.* **14**, 871 (2015).
 - [4] X.-L. Qi and S.-C. Zhang, The quantum spin Hall effect and topological insulators, *Phys. Today* **63**(1), 33 (2010).
 - [5] J. E. Moore, The birth of topological insulators, *Nature (London)* **464**, 194 (2010).
 - [6] M. Z. Hasan and C. L. Kane, Colloquium: Topological insulators, *Rev. Mod. Phys.* **82**, 3045 (2010).
 - [7] X. L. Qi and S. C. Zhang, Topological insulators and superconductors, *Rev. Mod. Phys.* **83**, 1057 (2011).
 - [8] J. E. Moore and L. Balents, Topological invariants of time-reversal-invariant band structures, *Phys. Rev. B* **75**, 121306(R) (2007).
 - [9] L. Fu, C. L. Kane, and E. J. Mele, Topological Insulators in Three Dimensions, *Phys. Rev. Lett.* **98**, 106803 (2007).
 - [10] X.-L. Qi, T. L. Hughes, and S.-C. Zhang, Topological field theory of time-reversal invariant insulators, *Phys. Rev. B* **78**, 195424 (2008).
 - [11] M. S. Bahramy, P. D. C. King, A. de la Torre, J. Chang, M. Shi, L. Patthey, G. Balakrishnan, P. Hofmann, R. Arita, N. Nagaosa, and F. Baumberger, Emergent quantum confinement at topological insulator surfaces, *Nat. Commun.* **3**, 1159 (2012).
 - [12] P. D. C. King, R. C. Hatch, M. Bianchi, R. Ovsyannikov, C. Lupulescu, G. Landolt, B. Slomski, J. H. Dil, D. Guan, J. L. Mi, E. D. L. Rienks, J. Fink, A. Lindblad, S. Svensson, S. Bao, G. Balakrishnan, B. B. Iversen, J. Osterwalder, W. Eberhardt, F. Baumberger, and P. Hofmann, Large Tunable Rashba Spin Splitting of a Two-Dimensional Electron Gas in Bi_2Se_3 , *Phys. Rev. Lett.* **107**, 096802 (2011).
 - [13] S. Hong, V. Diep, S. Datta, and Y. P. Chen, Modeling potentiometric measurements in topological insulators including parallel channels, *Phys. Rev. B* **86**, 085131 (2012).

- [14] C. H. Li, O. M. J. van't Erve, J. T. Robinson, Y. Liu, L. Li, and B. T. Jonker, Electrical detection of charge-current-induced spin polarization due to spin-momentum locking in Bi_2Se_3 , *Nat. Nanotechnol.* **9**, 218 (2014).
- [15] J. F. Tian, I. Childres, H. L. Cao, T. Shen, I. Miotkowski, and Y. P. Chen, Topological insulator based spin valve devices: Evidence for spin polarized transport of spin-momentum-locked topological surface states, *Solid State Commun.* **191**, 1 (2014).
- [16] J. Tang, L. T. Chang, X. Kou, K. Murata, E. S. Choi, M. Lang, Y. Fan, Y. Jiang, M. Montazeri, W. Jiang, Y. Wang, L. He, and K. L. Wang, Electrical detection of spin-polarized surface states conduction in $(\text{Bi}(0.53)\text{Sb}(0.47))_2\text{Te}_3$ topological insulator, *Nano Lett.* **14**, 5423 (2014).
- [17] Y. Ando, T. Hamasaki, T. Kurokawa, K. Ichiba, F. Yang, M. Novak, S. Sasaki, K. Segawa, Y. Ando, and M. Shiraishi, Electrical detection of the spin polarization due to charge flow in the surface state of the topological insulator $\text{Bi}(1.5)\text{Sb}(0.5)\text{Te}(1.7)\text{Se}(1.3)$, *Nano Lett.* **14**, 6226 (2014).
- [18] J. Tian, I. Miotkowski, S. Hong, and Y. P. Chen, Electrical injection and detection of spin-polarized currents in topological insulator $\text{Bi}_2\text{Te}_2\text{Se}$, *Sci. Rep.* **5**, 14293 (2015).
- [19] A. Dankert, J. Geurs, M. V. Kamalakar, S. Charpentier, and S. P. Dash, Room temperature electrical detection of spin polarized currents in topological insulators, *Nano Lett.* **15**, 7976 (2015).
- [20] L. Q. Liu, A. Richardella, I. Garate, Y. Zhu, N. Samarth, and C. T. Chen, Spin-polarized tunneling study of spin-momentum locking in topological insulators, *Phys. Rev. B* **91**, 235437 (2015).
- [21] J. S. Lee, A. Richardella, D. R. Hickey, K. A. Mkhoyan, and N. Samarth, Mapping the chemical potential dependence of current-induced spin polarization in a topological insulator, *Phys. Rev. B* **92**, 155312 (2015).
- [22] J. Tian, S. Hong, S. Sayed, J. S. Lee, S. Datta, N. Samarth, and Y. P. Chen, On the understanding of current-induced spin polarization of three-dimensional topological insulators, *Nat. Commun.* **10**, 1461 (2019).
- [23] A. Dankert, P. Bhaskar, D. Khokhriakov, I. H. Rodrigues, B. Karpiak, M. V. Kamalakar, S. Charpentier, I. Garate, and S. P. Dash, Origin and evolution of surface spin current in topological insulators, *Phys. Rev. B* **97**, 125414 (2018).
- [24] H. Cao, J. Tian, I. Miotkowski, T. Shen, J. Hu, S. Qiao, and Y. P. Chen, Quantized Hall Effect and Shubnikov-de Haas Oscillations in Highly Doped Bi_2Se_3 : Evidence for Layered Transport of Bulk Carriers, *Phys. Rev. Lett.* **108**, 216803 (2012).
- [25] H. Cao, C. Liu, J. Tian, Y. Xu, I. Miotkowski, M. Z. Hasan, and Y. P. Chen, Controlling and distinguishing electronic transport of topological and trivial surface states in a topological insulator, [arXiv:1409.3217](https://arxiv.org/abs/1409.3217).
- [26] See Supplemental Material at <http://link.aps.org/supplemental/10.1103/PhysRevB.103.035412> for the raw data of the spin signal of Bi_2Te_3 , electrical properties of Bi_2Te_3 and Bi_2Se_3 , as well as the control experiments on Bi_2Te_3 and Bi_2Se_3 . Also shown are calculated SHC over the entire energy range of the electronic structure of these materials.
- [27] F. Yang, S. Ghatak, A. A. Taskin, K. Segawa, Y. Ando, M. Shiraishi, Y. Kanai, K. Matsumoto, A. Rosch, and Y. Ando, Switching of charge-current-induced spin polarization in the topological insulator BiSbTeSe_2 , *Phys. Rev. B* **94**, 075304 (2016).
- [28] E. K. de Vries, A. M. Kamerbeek, N. Koirala, M. Brahlek, M. Salehi, S. Oh, B. J. van Wees, and T. Banerjee, Towards the understanding of the origin of charge-current-induced spin voltage signals in the topological insulator Bi_2Se_3 , *Phys. Rev. B* **92**, 201102(R) (2015).
- [29] Y. Xia, D. Qian, D. Hsieh, L. Wray, A. Pal, H. Lin, A. Bansil, D. Grauer, Y. S. Hor, R. J. Cava, and M. Z. Hasan, Observation of a large-gap topological-insulator class with a single Dirac cone on the surface, *Nat. Phys.* **5**, 398 (2009).
- [30] J. Sinova, S. O. Valenzuela, J. Wunderlich, C. H. Back, and T. Jungwirth, Spin Hall effects, *Rev. Mod. Phys.* **87**, 1213 (2015).
- [31] K. Kobayashi, Electron transmission through atomic steps of Bi_2Se_3 and Bi_2Te_3 surfaces, *Phys. Rev. B* **84**, 205424 (2011).
- [32] C. Şahin and M. E. Flatté, Tunable Giant Spin Hall Conductivities in a Strong Spin-Orbit Semimetal: $\text{Bi}_{1-x}\text{Sb}_x$, *Phys. Rev. Lett.* **114**, 107201 (2015).
- [33] G. Vignale, Ten years of spin Hall effect, *J. Supercond. Novel Magn.* **23**, 3 (2009).
- [34] H. Wang, J. Kally, C. Şahin, T. Liu, W. Yanez, E. J. Kamp, A. Richardella, M. Wu, M. E. Flatté, and N. Samarth, Fermi level dependent spin pumping from a magnetic insulator into a topological insulator, *Phys. Rev. Research* **1**, 012014 (2019).